Major role of water bodies on diurnal precipitation regimes in Eastern Africa.

Pierre Camberlin, Wilson Gitau, Olivier Planchon, Vincent Dubreuil, Beatriz M. Funatsu, Nathalie Philippon

Major role of water bodies on diurnal precipitation regimes in eastern Africa

Pierre Camberlin (1), Wilson Gitau (2), Olivier Planchon (3), Vincent Dubreuil (3),
Beatriz M. Funatsu (3), Nathalie Philippon (4)

(1) Centre de Recherches de Climatologie / Biogéosciences, UMR 6282 CNRS / Univ. Bourgogne Franche-Comté, 21000 Dijon, France

(2) Department of Meteorology, University of Nairobi

(3) LETG Rennes COSTEL / UMR 6554 CNRS / Univ. Rennes 2, 35000 Rennes, France

(4) Univ. Grenoble Alpes, CNRS, IRD, IGE, F-38000 Grenoble, France

International Journal of Climatology

Preprint version

Camberlin P., Gitau W., Planchon O., Dubreuil V., Funatsu B.M., Philippon N. 2018. Major role of water bodies on diurnal precipitation regimes in Eastern Africa. ***International Journal of Climatology***, 38, 2, 613-629

Abstract

Mean diurnal rainfall regimes over Eastern Africa (also referred to as the Greater Horn of Africa) are studied based on 3-hourly data from the TRMM 3B42 data set, averaged over a 17-yr period (1998-2014). The consistency with long-term mean raingauge data, available for partly independent periods, varies from good (Sudan, Ethiopia, Eritrea, Somalia) to very good (Kenya, Tanzania, Uganda). Over sea (Indian Ocean and Red Sea), the diurnal rainfall distribution is quite uniform; however, a morning peak dominates and there is evidence of offshore phase propagation south of the equator. Over land, both rainfall frequency and rainfall amounts show a dominant afternoon maximum (1500 to 1800 East African Time). However many inland regions show a delayed rainfall maximum (evening, nighttime or morning). The evening to nighttime maximum found over some land areas is associated with a phase propagation from areas showing an afternoon peak. This occurs west of high ground areas (Sudan and parts of the Great Lakes region) and in belts parallel to the seashores (Eritrea, northeastern Ethiopia, Somalia and eastern Kenya). The latter provide indirect evidence that sea breeze effects can be detected at unexpectedly great distances from the coast (up to 300-400 km) in parts of eastern Africa. A remarkable ring of early afternoon (1500) maxima is found around most lakes, although some east-west asymmetries occur. Over the lakes, a morning or late night maximum is mostly found. It is generally inversely related to the distance to the shorelines for the larger lakes, but over the mid-size lakes it is replaced by or competes with a late afternoon to evening maximum.

Key words

Horn of Africa, East Africa, Lake Victoria, Indian Ocean, rainfall, diurnal cycle, sea breeze, lakes

1. Introduction

The spatial distribution of rainfall over Eastern Africa is inherently complex. It is strongly controlled by terrain (Ethiopian and Kenya Highlands, East African Rift system) and water bodies (Indian Ocean and Red Sea to the east, and many lakes, including Lake Victoria, the world's second largest lake). These features interact with large-scale wind flows, resulting in local convergence / divergence and upslope / downslope circulation, all playing a major role on rainfall patterns (Beltrando, 1990 ; Mukabana and Pielke, 1996 ; Nicholson and Yin, 2002 ; Thiery et al., 2015 ; Cattani et al., 2016). These topographical features also influence the diurnal rainfall distribution, yet to date no comprehensive study has ever been carried out on this aspect for Eastern Africa as a whole.

In the tropics, land masses generally exhibit a strong afternoon maximum, associated with convection generated by daytime land surface heating (e.g., Meisner and Arkin, 1987 ; Yang and Slingo, 2001). Tropical oceans show more uniform diurnal rainfall distributions, although a nighttime or morning maximum often prevails (Hendon and Woodberry, 1993; Janowiak et al., 1994). Dai (2001) noted that over the tropical oceans, showery precipitation is most frequent from midnight to 0400 local solar time (LST), and maritime thunderstorms around midnight. Yang and Smith (2006) and Yang et al. (2008) noted that oceanic rainfall in convergence zones often shows a secondary late afternoon maximum besides the dominant late evening to early morning maximum. Nesbitt and Zipser (2003) noticed that over sea the morning maximum is due to more frequent mesoscale convective systems (MCS), whereas over land the MCS diurnal cycles vary significantly depending on environmental conditions. Non-MCS convection results in an afternoon peak, often triggered by relief. Over neighboring plains the afternoon maximum is not always prominent due to possible slope breezes and late drifts of major convective cells born over the highlands (Shinoda et al. 1999 ; Laing et al. 2008 ; Yaodong et al., 2008). Funatsu et al. (2012) observed that southern Amazonia convection is maximal near 1500 local time and minimal around 0700, with few significant differences between forested and deforested areas. Kikuchi and Wang (2008), distinguished three tropical diurnal cycle regimes. Both the oceanic regimes (small amplitude and early morning peak around 0600-0900 LST) and the continental regimes (large amplitude, afternoon peak around 1500-1800 LST) show little spatial phase propagation. By contrast the coastal regime shows a large amplitude and phase propagation of about 10 $m.s^{-1}$, both inland and offshore.

Regional and local studies on diurnal rainfall regimes over eastern Africa are few. Over Eastern Equatorial Africa, the only studies specifically dedicated to diurnal rainfall distribution were those by Tomsett (1975) and Asnani and Kinuthia (1979), using in situ rainfall records. They distinguished ten different diurnal patterns, strongly determined by the interaction between the synoptic scale flow and the mesoscale circulation induced by orography, like along the eastern slopes of the East African highlands and around Lake Victoria. The original diurnal regimes of Lake Victoria were actually noticed earlier by Flohn and Fraedrich (1966), who found that due to diverging lake breezes, the lake was cloudless at daytime, while the convergence of nocturnal land breezes accounted for a late night to early morning maximum in thunderstorm activity over the lake, slightly shifted westward by the large-scale easterlies. Analysis of cold cloud occurrences for 1983-1990 period confirmed the morning maximum of convective activity over Lake Victoria (Ba and Nicholson, 1998), in agreement with in-situ lakeshore rainfall data (Datta, 1981). An afternoon maximum is evident east of the lake.

Over Kenya, numerical simulations (Mukabana and Pielke, 1996) showed that differential heating and cooling of the terrestrial surface at day- and night-time between elevated and lowland areas, and between land and water bodies resulted in extensive breeze systems, contributing to rainfall regimes variations. Laing et al. (2011) noted that in equatorial Africa many MCSs form in the afternoon and move westward from the East African mountains. They also noted that along the Indian Ocean, a line of high cold cloud parallels the coast between 1400 and 1500 LST and moves inland in the evening. They attributed this pattern to land-ocean temperature contrast and associated breezes, but since it was at the margin of their study area it was not further analyzed. Along the Tanzania coast, Sumner (1982, 1984) documented the diurnal variations of breeze systems and their interaction with the monsoon. He found a late morning to early afternoon peak, shifted to the early morning during the northerly monsoon. Similar morning maxima are found on the Kenya coast (Okoola, 1978 ; Camberlin and Planchon, 1997).

In the northern part of Eastern Africa, diurnal rainfall variations are very imperfectly known, except for some studies of specific locations within the Ethiopian Highlands. Pedgley (1971) found a pronounced afternoon maximum both at Asmara in Eritrea (over 30% of rainfall occurrence from 1500 to 1800 local time) and Addis-Ababa in Ethiopia (where the rains are however more scattered across the day). The afternoon maximum also predominates further west over much of Sudan (Pedgley, 1969). However, in eastern Sudan, rainfall occurrence often peaks later at night or early morning, with a secondary maximum in the afternoon. Pedgley (1969) hypothesized that this could either be due to increased convergence within the Intertropical Convergence Zone (ITCZ), as a result of stronger nocturnal winds, or a relative afternoon subsidence over the Sudan plains connected to the strong convective activity over the nearby Ethiopian Highlands. The night maximum would therefore result from the westward drift of convective cells, embedded in the upper-tropospheric easterlies. In the Upper Blue Nile basin in Ethiopia, Haile et al. (2013) and Rientjes et al. (2013) compared hourly rainfall variations from CMORPH and TRMM satellite estimates to automatic weather stations for the year 2007. Both the rainfall occurrence and conditional mean rain rate were highest between 1500 and 1800 LST. Exceptions were found, especially in the Lake Tana Basin where a midnight and early morning maximum occurs. About 70% of the variance in the spatial distribution of nocturnal rainfall is explained by the distance to the center of Lake Tana (Haile et al., 2009).

Between the global or continental scale studies and the fragmentary ones carried out at local scale, there is a definitive lack of any study on diurnal rainfall regimes for the whole Eastern Africa. Yet, the complex patterns of land, sea, lakes and relief found across Eastern Africa (Fig.1) introduce many discontinuities in the land surface which generate daytime temperature gradients modulating atmospheric circulation and convective activity. In particular, it is unknown whether the morphology

of the coasts (bordered by mountain ranges along the Red Sea and Gulf of Aden, and by extensive plains south of Cape Guardafui) influences diurnal rainfall regimes.

The objective of this study is therefore to provide a broad-scale mapping of diurnal rainfall variations over Eastern Africa, also referred to as the Greater Horn of Africa (GHA). Rainfall regimes from satellite estimates are compared to in situ data of rainfall occurrence and rainfall amounts. Emphasis is put on the potential role played by water bodies (sea and lakes), both locally and remotely through sea/lake breezes. The study also explores diurnal phase propagation based on mean rainfall patterns. Section 2 presents the data (satellite estimates and in situ records) and the methods used to describe the diurnal cycles. Section 3 shows the general patterns of the diurnal peak rainfall (sections 3.1 and 3.2), then the specific contribution of water bodies (section 3.3). A discussion is provided in section 4.

2. Data and methods

The study makes use of the 3-hourly TRMM Multi-satellite Precipitation Analysis (TMPA) 3B42 rainfall data base (Huffman et al., 2007), version 7, at a 0.25° resolution. TMPA 3B42 (hereafter TRMM) is a multi-satellite product, incorporating microwave and infrared precipitation estimates, calibrated with monthly raingauge data, developed by the Mesoscale Atmospheric Processes Laboratory at NASA Goddard Space Flight Center. Version 7 improves upon previous versions of TRMM rainfall estimates by incorporating additional microwave and infrared data, revising the relationship between radar reflectivity and rainfall rates, the detection of surface clutter over high ground, and the use of better reference data bases for the passive microwave algorithm and the bias corrections (Huffman and Bolvin, 2013 ; Zulkafli et al., 2014).

Data are extracted for the period 1998-2014 and for the region from 28°E to 52°E and 12°S to 23°N (Fig.1). This covers the GHA, including Djibouti, Eritrea, Ethiopia, Somalia, Kenya, Uganda, Rwanda, Burundi, Tanzania, much of Sudan and South Sudan. 17-yr averages of 3-hr rainfall amounts and 3-hr rainfall occurrences are computed. The whole year is considered in the computation, since seasonal variations in diurnal rainfall phases are quite small (see supporting information S1 and S2).

TRMM data have been shown to reproduce quite efficiently observed spatial patterns and diurnal variations of rainfall in several parts of the tropics. For Western Africa, Pfeifroth et al. (2016) found that TRMM 3B42 rainfall estimates well captured the observed diurnal cycles of precipitation and their variability, with a slight delay (up to 2 hours) of evening peak precipitation. For Eastern Africa, TRMM 3B42 was found to perform very well in reproducing rainfall patterns (Cattani et al., 2016). With

regards to the diurnal cycles, a validation has been made only over the Lake Victoria and upper Blue Nile areas, where a good agreement exists with ground observations (Haile et al., 2013).

Comparisons are made with early published data of in situ mean hourly rainfall occurrence in Sudan, Eritrea and Ethiopia (Pedgley 1969 and 1971), mainly for the period 1951-1966. Three-hour station data from these studies are resampled to match the TRMM time sampling. For Kenya, Uganda and Tanzania, mean percentage hourly distribution of rainfall amounts at a number of stations are obtained from Tomsett (1975), averaged over 6 to 26 years, mostly in the 1950s and 1960s. For northern Somalia, hourly rainfall data are collected from 5 automatic weather stations set up as part of the Somalia Water and Land Information Management (SWALIM) project. They cover 2 to 5 years within the period 2008-2015. Three-hour averages of rainfall amounts matching the TRMM time sampling are computed for the Kenya, Tanzania, Uganda and Somalia stations.

All times are expressed in East African Time (EAT, i.e. GMT+3). In the notations below, 0300 refer to the 3-hr period from 0130 to 0430 EAT, 0600 to the period from 0430 to 0730, and so on. Phase variations are investigated by mapping the timing of precipitation maximum and by showing time-space plots of 3-hr frequencies of rainfall occurrences or 3-hr mean rainfall amounts. A comparison between mean diurnal rainfall regimes for land and lake areas is done to infer the influence of the latter on rainfall distribution, and its dependence to the size of the lakes. Additionally, composite diurnal rainfall regimes are plotted as a function of the distance to the coastline to detect propagative features possibly associated with sea breezes.

3. Results

3.1 Diurnal rainfall phases

The diurnal rainfall patterns are first documented by plotting the 3-hr period during which the rainfall is most frequent (as a number of observations with rainfall of at least 1 mm) (Fig.2a) and the 3-hr period which records the highest mean rainfall amounts (Fig.2b). The two maps are quite similar, hence they will not be discussed separately.

Over land, diurnal rainfall regimes show a dominant peak in the early or late afternoon (1500 or 1800 EAT), suggesting an effect of daytime convection as over many other tropical land areas. The early afternoon maximum is mostly found (1) in a narrow belt along the coast (up to about 100 km inland, suggesting a relationship with sea breezes, see below), (2) close to some lake shores (e.g., in the periphery of lake Tanganyika), (3) in inland depressions far from the coast (e.g., in a crescent south of the Ethiopian Highlands) and (4) marginally over isolated mountain peaks. The late afternoon

maximum is more widespread. For the region as a whole, 41.5% of the land grid-points show a maximum rainfall occurrence at 1800 EAT (Fig.2, central histogram). Over the Indian Ocean, an early morning peak generally prevails (often at 0600), but the amplitude of the diurnal cycle is much smaller than inland (coefficient of variation around 2-6%, as against 7-15% over most land areas, see also supporting information S3).

However, there are 3 main discrepancies from this general pattern:

(i) Large inland areas, at some distance from the coast, exhibit a nighttime maximum (red to dark blue colours on Fig.2). Mainly located in lowland areas or gently sloping plateaus, they include northern Sudan, northeastern Ethiopia, parts of inland Somalia and east-central Kenya.

(ii) A few inland areas, like over the ocean, display a late night / early morning maximum (0600 to 0900): some areas southwest of the Ethiopian Highlands, Lake Victoria and Lake Tanganyika. Other lakes often singularize by their regimes, with an evening or nighttime peak. An asymmetry is also obvious between lakeshores, especially for Lake Victoria where an afternoon peak dominates along the eastern shores, shifting to a morning one on the western shores (see also Lake Tanganyika and Lake Turkana).

(iii) Over sea surfaces, the early morning peak is often delayed to 0900 or 1200 close to the coast (Red Sea and Gulf of Aden, Tanzania and Kenya coasts), although caution should be exerted over coastal areas due to the fact that TRMM rainfall estimates use different algorithms over land and sea (McCollum and Ferraro, 2005), and the diurnal amplitude is small over the ocean. Further offshore, the area 200-600 km off the Tanzania coast is an exception by showing an afternoon maximum.

Interestingly, there are several instances of apparent long-distance phase propagations of the diurnal signal from the coastlines (arrows on Fig.2). A westward propagation (arrow A) is evident from the Eritrean coast to northern Sudan (early afternoon maximum along the coast, shifting to 1800 west of the highlands), then to the night over the Nile plains, (over a distance of about 400-600 km). Similar shifts from 1500 to 0300 occur:

- southwestward from the Red Sea coast in eastern Eritrea to central Ethiopia, over about 500 km across the Afar depression (arrow B);

- in Somalia and Kenya both southward from the Gulf of Aden (arrow C) and northwestward from the Indian Ocean coast (arrows D & E), over distances of 300 to 500 km.

Less clear phase propagation can be found further inland, mainly from east to west, e.g. from central Ethiopia to South-Eastern Sudan (arrow F), or from the Western Kenya Highlands to Lake Victoria and

then Rwanda (arrow G). Note that over the southern part of the Indian Ocean sector there is an apparent propagation of the rainfall phase both offshore and onshore.

A zoom on 3 regions (northwestern GHA, Equatorial GHA, and Somalia) enables a comparison with in situ data and a preliminary discussion of possible mechanisms. Note that the spatial sampling of in situ data is not fully satisfactory, with more stations in regions showing an afternoon peak. In northwestern GHA (western Ethiopia, Eritrea, Nile plains, Fig.3), there is a fair agreement between in situ records of the time of most frequent rainfall occurrence published by Pedgley (1969 and 1971 ; blue lines on side panels) and TRMM data (bars). Correlations between in-situ data and TRMM are statistically significant (P=0.95) at 56% of the stations, excluding En-Nahud and Kosti where the diurnal cycle is quite flat. An afternoon maximum dominates, especially over the Ethiopian and Eritrean highlands, generally peaking at 1800 or sometimes earlier (Asmara and Addis-Ababa, panels 10-11). Valleys make an exception (e.g. along the Blue Nile from Lake Tana, where the phase is often delayed to 2100). This likely reflects the development of daytime convective cells over elevated ground and their later shift to the valleys, as noted by Rientjes et al. (2013). A conspicuous feature is that the maximum rainfall occurrence is delayed to the night over much of the northern Sudan plains (e.g. Khartoum, panel 1), in agreement with Pedgley (1969). The apparent propagation suggests a westward drift of the MCS developed from daytime convection over the Eritrean and Ethiopian highlands, as a result of the upper-tropospheric summer easterlies (see supporting information S4). This is also found further south, although the night maximum is often masked out by the afternoon peak which becomes dominant in the Nile plains south of 12°N. At Kosti (13°N, panel 4) there is a double peak where the afternoon maximum is not strong enough to override the nighttime maximum. Dots on figure 3 show a secondary afternoon maximum over much of the northern plains, suggesting daytime convection combined to MCS drifts from the highlands. This propagative signal can actually be tracked back to the Red Sea coast, with an early maximum (1500) possibly associated with the sea breeze front.

Over equatorial GHA (Fig.4), where the pattern of terrain and waterbodies is very complex, TRMM mean 3-hr percentage rainfall amounts are in excellent agreement with in situ data from Tomsett (1975) although the periods for calculating the mean regimes are completely different. Correlations between in-situ data and TRMM are statistically significant (P=0.95) at all the 18 stations (average correlation: 0.91). A late afternoon maximum (1800) again dominates over land. This 3-hr period often accounts for a very large proportion of the daily rainfall amounts, exceeding 35% in pixels with a plus sign on figure 4 (e.g., Kisumu, panel 5). The peak rainfall is found earlier (1500) at the periphery (mainly to the west) of water bodies, including both the Indian Ocean (in a 100 to 150-km wide inland corridor) and many of the lakes, for instance to the west of lakes Victoria, Albert, Edward and Malawi/Nyassa, and all around Lake Tanganyika. The early afternoon peak is also found in northern Kenya (except over

Lake Turkana) and over or slightly west of high ground areas, e.g. above 1400 m in Tanzania and near Mt Kenya (Nanyuki, panel 12). The location of these early afternoon rainfall maxima suggests an interaction between topography and the mid-tropospheric easterly flow, dominant during the main rainy seasons (March-May and October-December, see supporting information S4). However, in two types of regions the afternoon maximum does not prevail:

(i) Over the water bodies themselves (lakes, Indian Ocean in a 150-km wide alongshore corridor), early morning maxima dominate (0600 or 0900). Along the coastline and some western lakeshores the peak is often delayed to 1200, like in Malindi, Mombasa and Dar-es-Salaam (panels 15, 17, 18). Reciprocally, the peak occurs earlier (0300) over the eastern part of Lake Victoria, southeastern part of Lake Tanganyika and northeastern parts of Lake Malawi/Nyassa.

(ii) A few inland areas display evening or nighttime maxima. This is most obvious across eastern Kenya, showing belts parallel to the Indian Ocean where the rainfall phase is gradually delayed as the distance from the ocean increases. This pattern is absent further south in Tanzania. More scattered evening peak areas are found in central Tanzania and northern Uganda (Lake Kyoga area south of Gulu, panel 2). They are mainly located in depressions or to the east of mountain ranges. It is suggested that daytime convection is detracted by nearby ascending slope breezes, and that the maximum results from the advection of convective systems developed in the afternoon further east.

Finally, figure 5 provides a zoom on the Somalia peninsula. There is a fair agreement between TRMM and the SWALIM automatic in situ rainfall recordings (side panels), with an average correlation of 0.77 (significant at P=0.95) when we exclude Galcaio (panel 5) where the in-situ record is very short (2 years) and the rainfall very low (150 $mm.yr^{-1}$). The resulting diurnal pattern is quite simple: an early afternoon maximum prevails alongshore, in a 100 to 150-km wide strip. Further inland the phase shifts to the late afternoon (e.g. at Borama, Hargeisa and Burao, panels 1-3), then to the evening and the night as ones moves away from the coast. A broad area of early morning peak (0300) is found in Ogaden (eastern Ethiopia) and southern Somaliland, and the maximum is even found as late as 0600 near 6°N-44°E, 450km from the coast. The pattern, more or less parallel to the coasts, suggests that the diurnal cycle could be controlled by a propagation of sea breeze fronts from both the Gulf of Aden, in the north, and the Indian Ocean in the east. The inland nighttime maximum often cohabits with an afternoon one, weak (Garowe, panel 4) or occasionally stronger like further south (5°N-44°N).

3.2 Maps and cross-sections of 3-hour rainfall occurrence

In order to better show the distribution of rainfall within the day, 3-hourly maps of mean rainfall occurrence have been plotted (Fig.6). Rainfall occurrence is at its lowest at noon. It strongly increases at 1500 EAT. The areas of most frequent rainfall occurrence are clearly co-located with the main

mountain ranges, suggesting their role on daytime convection. At 1800 convective cells become bigger and/or drift (in slightly different directions depending on the large-scale flow), with rainfall occurrence exceeding 15-20% over highland areas. Later in the evening (2100) and at night (2400 and 0300), the areas of high rainfall occurrence generally shift westwards and gradually decay. The wet area in the southwestern Ethiopian Highlands makes an exception for it is still very active at night, though also showing a westward drift towards the nearby plains in the following morning. Lowlands are quite dry, except in southern Tanzania, South Sudan and at a small distance of the coast in Kenya and southern Somalia. A line of medium rainfall occurrence (5 to 9%) parallel to the east African coast actually develops at 1200 and moves inland during the afternoon and evening, gradually decaying. The main lakes, especially Lake Victoria, show a markedly different cycle. They are generally rain-free in the afternoon, but a strong maximum develops in the second part of the night and the morning. Over the Indian Ocean, there is much less diurnal variation than over land. However, rainfall occurrence generally peaks in the morning as discussed above, with a secondary maximum off the coasts of Kenya and Tanzania around 1500.

As a way to mask out spatial variations in mean rainfall amounts (e.g. between the drier lowlands and wetter highlands), figure 7 displays rainfall occurrences for each 3-hr period as a percentage of all local rainfall occurrences. This better shows the generalized pattern of propagative rainfall lines from the Indian Ocean and Red Sea coasts (at 1200) to the interior. This apparent propagation can be tracked till 0300-0600 in some inland areas of Kenya and Somalia, and from the Red Sea towards the Nile Valley in northern Sudan. Propagation is also evident over Lake Victoria from the eastern to the western shore from 0300 to 1200.

Two time-longitude plots are drawn to further analyze the propagative patterns and their relationship with terrain.

The first plot (1.5°S, Fig.8), between the Indian Ocean and the Western Rift Valley, emphasizes the contrast between the uniform distribution of rainfall occurrence over the ocean and that found over land areas and Lake Victoria. Areas over and to the west of the highest ground (Western Rift, 29.5°E, and Western Kenya Highlands, 35.5°E) display the characteristic afternoon rainfall maximum. Evidence of downwind (westward) propagation is found. Afternoon maxima (slightly earlier) are also found west of Lake Victoria (31°E) and near the Indian Ocean coast (41°E), from where the phase is similarly delayed as one moves westwards, generating a nighttime maximum near 38°E. However it appears that this maximum results from an (apparent) propagation from both the east (Indian Ocean coast) and the west (Central Kenya highlands). Different phase speeds on either side of 39°E also suggest different mechanisms, possibly sea breeze front displacement to the east and convective cells

movement to the west (see discussion below). The morning maximum of Lake Victoria (32°E) is distinctive. In this sector, a westward drift is also conspicuous, possibly in continuity with the convective systems developed in the Western Kenya Highlands in the afternoon, drifting westward and then reactivating over Lake Victoria in the early morning. Some systems might even propagate further west over the Western Rift Highlands where daytime convection may rejuvenate them. However, the different apparent phase speeds (4.1 and 9.9 $m.s^{-1}$ respectively) suggest different mechanisms, or propagations in different directions.

The second plot (15°N, Fig.9) depicts the Red Sea- Eritrea- Sudan area, again with strong evidence of the effect of relief on rainfall timing. Highlands on both sides of the Red Sea (over 2000 m in Eritrea and Yemen) display an overwhelming afternoon maximum (1500 to 1800 EAT), with no rain at all between 0300 and 1200. The later maximum on the Yemenite side (1800 as against 1500 for the African side) could be due to a later exposition to the sun's rays, delaying slope breezes, or to different interactions between breezes and mid-tropospheric winds. Convective systems developed over Eritrea clearly shift westward (at about 10 $m.s^{-1}$), resulting in a strong maximum around midnight at 36°E on the foothills. Further west, the nighttime maximum is still obvious, but a large share of rainfall occurs at other times of the day, and there is no more evidence of a propagation, suggesting other mechanisms are at work. In sharp contrast with the highlands, the (dry) Red Sea shows a weak double peak regime, with morning rainfall typical of many maritime areas, and an evening peak likely resulting from the drift of systems developed in the highlands. For the Yemen highlands, rain structures propagate both westward and eastward.

3.3 Role of waterbodies on land diurnal rainfall regimes

A closer attention is paid to the role of water bodies (first maritime areas, then lakes) on the diurnal rainfall distribution, both over these surfaces and over the nearby land areas. Figure 10 shows the mean frequency of 3-hr rainfall occurrence (relative to the local total rainfall occurrence) over the continent, as a function of the distance to the nearest maritime coastline, all latitudes combined from 12°S to 23°N. Two diurnal cycles are displayed for legibility, and three months are retained in addition to the yearly average to detect possible seasonal changes. For all plots, a remarkable pattern is shown where, starting from the vicinity of the coast, rainfall occurrence is low before 1000 EAT, then rapidly reaches a mid-afternoon maximum (1500) followed by an almost as rapid decrease (rainfall occurrence <12% well before 2100). A similar pattern is found further inland, but with a gradual delay such that the maximum occurs at 1800 at 50-150 km from the coast, 2400 at 250-300 km, 0300 at around 300-400 km, and is still faintly visible at 0600 beyond 400 km from the coast. The switch to drier conditions later in the day is very clear, with a constant propagation rate (7-8 $m.s^{-1}$) in April and October, the main

rainy seasons in Somalia and Kenya, from the coast to at least 300 km inland. Beyond 250-300 km from the coast, in April and October, the nighttime maximum resulting from this propagative feature coexists with a local afternoon maximum (1500-1800), which becomes dominant beyond about 400 km. This pattern evidently points to two different mechanisms accounting for diurnal rainfall variations: local convection driven by daytime surface heating, and rainfall activity along the sea breeze front, whose inland penetration can be associated with the sharp late afternoon rainfall decrease close to the coast, then gradually later inland. If the propagative pattern shown on figure 10 can be interpreted as a result of sea breeze penetration, it points to a very deep (and unexpected) effect inland (see discussion in section 4).

The analysis now considers inland water bodies. East African lakes of different sizes have been selected, ranging from 230 km^2 for Lake Manyara to 68 800 km^2 for Lake Victoria (Fig.11). Their mean diurnal regimes (in $mm.hr^{-1}$, bars on the left panels) are plotted individually and as an average for all East African lake pixels (bottom right panel). In the computations, mixed land-lake pixels (at least 25% of water) have been included. For the largest lakes the computation has also been done for the full lake pixels (>75% water). However, the results being similar for the two thresholds (Fig.11), the regimes will not be discussed separately. A morning maximum is obvious for the largest lakes only (Victoria, Tanganyika, both at 0900). Over the northern part of lake Malawi (Nyassa), it is slightly earlier (0300 to 0600), as for other elongated, narrow Rift lakes such as Rukwa and Albert (see discussion below). For the smaller lakes, an afternoon maximum appears, giving double-peak regimes (Eyasi, Manyara, Ziway, Abaya, and even the larger Lake Turkana) or almost single-peak regimes (Edward, Tana, Kyoga, Kivu). In these cases, the afternoon maximum is late compared to other inland areas, or even shifted to the evening (e.g., Lake Kyoga). The spatial average, dominated by the Great Lakes (especially Lake Victoria) confirms the inverted patterns between land and lake regimes, with the dominating morning maximum for lakes contrasting with the afternoon one for land (dashed line with squares).

Since the lake size seems to matter, lake pixels are now stratified according to their distance to the nearest lakeshore (Fig.12). 3-hr rainfall amounts for sea and land pixels are also plotted for comparison. At 0300, there is little effect of the distance to the lakeshore. The contrast with the land pixels is small as well. At 0600, while rainfall decreases over the land, it strongly increases over the lakes at more than 80 km from the lakeshores. The gradient further increases at 0900, and is still strong at 1200. A dramatic change occurs at 1500: while rainfall away from the shores collapses, it increases over land. Areas close to lakeshores start to be affected by the rainfall increase from 1800. This pattern persists in the early night, gradually weakening. These results, especially the quick transition between 1200 and 1500, suggest that local circulations, whose strength and extent are related to the lake size, are instrumental in shaping the diurnal regimes over the lakes. While the cooler surface of the lakes is

detrimental to convection during the day, the drift of systems generated over nearby land areas can explain the frequent early evening maximum on the shores (cf. also figures 2-3). As discussed above, given the east-west asymmetries related to interactions between breezes and synoptic-scale winds, this analysis could be further refined by separating eastern and western lakeshores.

On the whole, evidence is found of two types of lake regimes: a late afternoon regime, associated with the propagation of convective systems from non-lake areas, mostly over small lakes and lakeshores, and a late night to morning regime, restricted to the larger lakes, associated with a nighttime convergence and uplift over the lake surface.

4. Discussion

TRMM 3-hourly data show that GHA land areas, as in most other tropical regions, generally exhibit a clear afternoon maximum (at 1500 or 1800 EAT), explained by the predominant convective rains and their initiation by daytime surface heating.

However, it is noteworthy that extensive areas depart from this pattern. Although some of these peculiar features have been shown in earlier studies based on a few station records, several new patterns are revealed and are now discussed for a more complete interpretation.

(1) Role of the sea-land interface on diurnal rainfall regimes

One of the key findings is the major role of the sea-land interface as a determinant to diurnal rainfall variations in the GHA, not only along the coast but at a long distance from it. This is evident in the gradual delay in the rainfall maximum from the early afternoon to the evening and sometimes the night hours as one moves inland. It is suggested to reflect the inland progression of the sea breeze and associated convective activity along the breeze front, as documented before in other tropical regions (Carbone et al., 2000 ; Mori et al., 2004 ; Zhou and Wang, 2006 ; Kikuchi and Wang, 2008). This feature has never been shown earlier for the GHA, for which little information is available on sea breezes and their role on rainfall regimes. Previous studies point to a morning precipitation maximum at coastal stations of Kenya and Tanzania (Asnani and Kinuthia, 1979 ; Sumner, 1984 ; Camberlin and Planchon, 1997). Our study shows that the coastal morning peak quickly shifts to an early afternoon peak a few kilometers inland. The morning peak is generally attributed to the onset of the sea breeze. Then its subsequent penetration over the continent, as the land surface heats up, results in progressively later rainfall peaks. The orientation of the coastline with respect to dominant winds is important (Sumner, 1982). The inland propagation along much of the Tanzanian coast, where the winds often parallel the coast (supporting information S4), is limited to the afternoon hours (Fig.2).Further north in Kenya and

Somalia, where winds during the rainy seasons are onshore and orthogonal to the coastline, the phase propagation extends further inland into the night, suggesting a deeper sea breeze penetration.

In the Red Sea area, previous studies on sea breezes are even scantier. In summer along the Sudanese coast, WRF simulations show an afternoon sea breeze of 3-8 $m.s^{-1}$, replaced at night by a land breeze (Davis et al., 2015). Our results indicate that the sea breeze penetration is likely to explain the progressive delay in the rainfall phase from the coastline to the interior in the Afar region, and south of the Gulf of Aden. Further north in northern Eritrea and Sudan, it is uneasy to separate the westward drift of afternoon convective storms initiated over the highlands, from the effect of the sea breeze penetration (similarly westwards).

The rainfall phase propagation from the coast raises the question of the maximum inland extent of sea breezes in the GHA. In Kenya, Nganga and Masumba (1988) detect them 120 km away from the coast. Our study suggests that their penetration reach 300-500 km from the coast in Eritrea, the Afar region, Somalia and eastern Kenya. This is not at odds with numerical and observational results over various tropical regions. In the Guianas and around the Amazon delta, the sea breeze penetrates up to at least 100 km inland (Snow 1976; Molion 1987). In north-eastern Brazil, sea-breeze fronts identified by remote sensing at the warmest time of the day penetrate up to 100 km inland during the late dry season, because of high land–sea temperature differences (Planchon et al., 2006). In Saudi Arabia, the strong desert heating results in a deep inland penetration of the sea breeze of over 225 km (Steedman and Ashour, 1976). Sea breeze penetrations of 250 km were reported in Pakistan (Holmes, 1972), and of over 200 km in flat areas of Australia (Physick and Smith, 1985 ; Planchon, 1995), with possible penetrations of up to 500 km (Clarke, 1984 ; Garratt and Physick, 1985). South of the Persian Gulf, Zhu and Atkinson (2004) obtained a simulated penetration of over 250 km. Over Sumatra Island, Mori et al. (2004), using TRMM data, found both offshore and onshore propagations of diurnal rainfall phases. The onshore propagation, substantiated by upper-air dynamics, can be tracked over 400 km, with a peak rainfall at 1500 LST near the coast, gradually delayed to 0600 in the east.

Several factors support a deep inland penetration of sea breezes in the GHA: (i) the low latitude, which restricts wind deviation due to the Coriolis force ; (ii) the relatively flat surfaces, at least over southern Somalia, eastern Kenya and the Afar depression; and (iii) the strong sea-land temperature contrast : maximum temperatures over northeastern Kenya are in the range of 33-37°C during the rainy seasons, while the coastal Indian Ocean reaches 27-29°C. A land-sea temperature gradient over 5°C is required for a deep sea breeze penetration (Miller et al. 2003). The smaller effect of the Coriolis force makes this threshold even lower (4°C) in the tropics (Okoola 1978; Cautenet and Rosset 1989), as against 6°C at higher latitudes. The deep inland phase propagation is also suggested to result from both advection

processes due to large-scale circulation and mesoscale gravity currents (Clarke, 1984) generating a new convergence ahead of the initial cloud system.

Over the open sea bordering East Africa, while the diurnal distribution of the rains is more uniform, there is evidence of offshore propagation. This is mostly south of the equator, with a 50-km wide coastal belt showing a morning peak (0900) then a mid-afternoon peak (1500) further offshore, as plausibly related to land breezes then gravity waves propagation. We hypothesize that the better developed offshore propagation south of 3°S results from both the warmer sea surface temperatures and the direction of the prevailing winds, crossing the seashore at a small angle. Further north off the Southern Somalian coast, the predominantly onshore winds during the rainy seasons (supporting information S4, March-May and October-December) are detrimental to land breezes. Offshore phase propagations were found in many tropical regions, including Indonesia (Mori et al., 2004 , Teo et al. 2011) the Bay of Bengal, Central America and West Africa (Yang and Slingo, 2001 ; Biasutti et al. 2012).

(2) Other nighttime inland maxima

Many nighttime maxima can be related to rainfall systems associated with sea breeze propagation, as discussed above, but some cases exist of other mechanisms. Instances of a nighttime maximum have been found in other inland tropical regions, such as southwestern Amazonia (Rickenbach, 2004), the Himalaya (Sahany et al., 2010) and the Khorat Plateau in Thailand (Takahashi et al., 2010). In the Amazonian case, a post-midnight secondary maximum was attributed to nocturnal convective events, many of which are traced to squall lines propagating westward thousands of kilometers from their origin, i.e. the sea breeze front developed in northeast Brazil (Kousky, 1980; Garstang et al., 1994 ; Machado et al., 2014). The late night/early morning peak over the Himalaya foothills was suggested to be associated with the convergence of katabatic winds and the southwesterly monsoon (Sahany et al., 2010). We consider that these two mechanisms also operate in the GHA.

Nighttime maxima observed in northern and central Sudan clearly result from the westward shift of MCS generated over the Ethiopian and Eritrean Highlands. This was suggested by El-Fandy (1949) and Pedgley (1969), then confirmed by Desbois et al. (1988). South Sudan is similarly affected, but in-situ convective systems also develop which result in a dominant afternoon rainfall peak (section 3.1). Laing et al. (2008) actually found that the lee of the Ethiopian Highlands, east of 31°E, was the birthplace for 25% of cold cloud streaks occurring over Northern tropical Africa between 5 and 15°N. A nighttime to early morning maximum is also found over southeastern Sudan, northwestern Kenya (around Lake Turkana) and nearby Ethiopia. It results either from the drift of MCS generated over the Southern

Ethiopian Highlands (as suggested by the phase propagation from the north-east) or from the nighttime convergence of katabatic flows from the Ethiopian and Kenya-Uganda Highlands.

Further south, Asnani and Kinuthia (1979) found that stations on the eastern slopes of the Kenya and Tanzania Highlands, like Nairobi, had a nighttime maximum, instead of the usual late afternoon one as expected inland. As discussed above, this nighttime maximum may partly be related to convective systems generated along the sea breeze front and later advected further inland. However, Asnani and Kinuthia (1979) suggested that it was rather a result of the downslope flow opposed to the easterly tradewinds. It is safe to consider that the two mechanisms either combine (convergence between katabatic winds and the easterly flow, possibly reinforced by the sea breeze) or operate at different times to explain the nighttime maximum. The January pattern (Fig.S2a), in which southern Kenya shows a discontinuity between the diurnal phase associated with a propagation from the coast, and the nighttime maximum northeast of Mt Kilimanjaro and southeast of Mt Kenya, actually suggests that katabatic winds are an important player.

(3) Role of inland water bodies and lake breezes

The largest East African lake, Lake Victoria, is known for its specific diurnal cycle of precipitation (Flohn and Fraedrich, 1966 ; Datta, 1981 ; Ba and Nicholson, 1998 ; Nicholson and Yin, 2002). Nicholson and Yin (2002) found similarities over Lake Tanganyika. TMPA 3B42 data confirmed a strong morning peak over these two lakes. Several other large- and medium-size lakes in the region exhibit a nighttime or morning maximum. Numerical climate modeling of the East African Great Lakes region (Thiery et al., 2015) found precipitation occurring mostly at night and morning hours over the lakes (0300-1200 EAT), in agreement with our results. However, the precipitation maximum they found for the surrounding land, around local noon (1000-1500) is too early and fits neither TRMM nor in-situ observations.

Except for the smallest lakes, the share of morning and late night rainfall is proportional to the distance from the lakeshores, a feature consistent with observations by Haile et al. (2009) for Lake Tana (Ethiopia). The lake surface remains cool in the afternoon while convection develops over the heated surrounding land areas. The lake breeze which develops results in subsidence over the lake, thus promoting dry conditions. This has been well shown for Lake Victoria (Flohn and Fraedrich, 1966; Anyah et al., 2006; Thiery et al. 2015), but it may also apply to large lakes such as Lake Tanganyika over which strong diurnal wind changes are found. However, Lake Tanganyika being a Rift lake, about half of its diurnal wind variation is due to slope breezes, and one quarter is strictly due to the thermal lake effect (lake breeze) (Savijärvi, 1997). East of Lake Victoria, strong interactions exist with the slope

winds of the nearby highlands (Kayiranga, 1991; Anyah et al., 2006; Thiery et al. 2015). West of the lake, the afternoon lake breeze also combines with slope winds (Dhonneur, 1985) to explain the mid-afternoon maximum, then the late afternoon peak further west, as the breeze front shifts westward, aided by the large-scale easterlies. A similar combination occurs in the Spanish eastern Pyrenees (Llasat and Puigcerver, 1997) where combined sea and slope breezes enhance convection. The late night / early morning rainfall maximum is explained by the instability over the relatively warm lake, enhanced by the converging land breezes.

Over small-size lakes, such a convergence may be too weak to generate a rainfall peak. The diurnal regime is therefore characterized by an evening maximum resulting from the drift of convective systems generated over the nearby land areas. Crosman and Horel (2010) noted that while lake breezes associated with large lakes (d > 100 km) have similar characteristics to sea breezes, this does not apply to small water bodies due in part to shoreline curvature effects. A bimodal regime, including both a morning peak and an afternoon peak, was found over several relatively small east African lakes (e.g., Abaya, Ziway, Eyasi, Manyara, which cover between 250 and 1150 km^2). This sharp morning maximum, given the small size of these lakes, is puzzling. Although Tian and Peters-Lidard (2007) in the USA reported systematically-positive errors in TRMM 3B42 (version 6) over inland water bodies, this was not confirmed by Paiva et al. (2011) for Amazonia where relatively small water bodies (rivers) exhibit specific diurnal regimes (lowest rainfall during the afternoon, highest at night and early morning), opposite to those of land areas. Medium-size lakes such as Malawi, Rukwa and Albert show a nighttime (0300 EAT) maximum (Fig. 11). Their small width, compared to Lake Victoria and Tanganyika where the maximum occurs at 0900, makes the nighttime convergence of land breezes less durable, with a faster cooling of the lake surface than over bigger lakes.

As a result of the dominant easterly winds over much of the Great Lakes region, a notable feature is the asymmetrical pattern of the phase of diurnal rainfall regimes around the main water bodies. The nighttime-morning maximum is deflected westwards of the lake surface. This is conspicuous for Lake Victoria (Anyah et al., 2006) but it is also visible over Lake Tanganyika, Rukwa, Malawi, Albert and Turkana (Fig.2). For Lake Tanganyika, late night to early morning convection is frequent along the western lakeshore (Nicholson and Yin, 2002).

5. Conclusion

This study highlighted the potential of 3-hourly rainfall estimates from the TRMM 3B42 product, which compare favorably with independent in-situ data, to document the patterns of diurnal precipitation

variations in eastern Africa. Maps of the diurnal rainfall phase based on 17-yr (1998-2014) averages show evidence of an important spatial complexity strongly controlled by geographical features (orography and water bodies), with relatively little seasonal changes. Besides a confirmation of the role of relief and Lake Victoria on diurnal regimes, the study provided for the first time evidence of a strong diurnal modulation of the rains in areas never investigated before, such as Somalia and the eastern part of Ethiopia.

Over the region as a whole, 70% of the annual rainfall amount falls between 1330 and 0130 over land areas (lake surfaces excluded). Land surfaces display an overwhelming afternoon maximum, with a late afternoon peak (1800 EAT) at 41.5% of the pixels. The phase occurs slightly earlier (1500) along land strips (about 100-km wide) bordering most of the Indian Ocean coast as well as many of the Great Lakes, as shown by rings of mid-afternoon maxima around most water bodies. This suggests a key role of the daytime sea and lake breezes in controlling convection over these regions. Reciprocally, the phase is delayed to the evening or even nighttime hours in some regions further inland such as eastern Ethiopia, northeastern Kenya, the Afar depression and the northern Nile plains. The gradual delay in the rainfall phase from the coast to the hinterland, most developed in lowland areas, sometimes at unexpectedly long distances from the coast (300-500 km), is likely associated with sea breeze propagation combined, in some regions, with downslope winds. Propagating mesoscale systems developed over high ground areas during the afternoon, also account for the late (nighttime) maximum found in a few parts of the GHA, like northern Sudan.

The diurnal rainfall distribution over the Indian Ocean and the Red Sea is much more uniform. However, a morning peak dominates close to the coast (and at some coastal locations), especially south of the equator. Phase propagation is evident south of 3°S, resulting in a weak afternoon maximum further offshore. Lakes themselves demarcate from land surfaces by their diurnal regimes. The larger ones (Victoria, Tanganyika, Malawi/Nyassa) show a dominant late night / early morning maximum, more evident as the distance to the lakeshore increases. It was shown in previous studies to be related to nighttime convergence of land breezes over the relatively warm lake surfaces, possibly aided by downslope breezes. It is found that smaller lakes also display specific diurnal regimes: a morning peak frequently combines with a late afternoon one resulting from the propagation of convective cells generated over the surrounding warmer land areas. Further work, considering the actual propagation of cloud systems or the use of limited area climate modelling, is required to fully assess the mechanisms explaining the phase shifts in diurnal precipitation regimes from the coastlines or the highlands and the interaction between sea-land-lake breezes and the large-scale winds.

Acknowledgements

This article is dedicated to the memories of Raphael Okoola (1943-2016) and Gérard Beltrando (1956-2016) for their contributions on the climates of East Africa.

Supporting information

Appendix S1: Seasonal variations of diurnal rainfall phases

Figure S2: Diurnal phase of peak rainfall in Eastern Africa for the months of January, April, July and October. Areas left blank are those where mean rainfall is less than 0.02 $mm.hr^{-1}$ (about 15 $mm.mth^{-1}$) or where the maximum 3-hr rainfall does not exceed 17% of the monthly total. Solid lines: 1000 (white) and 2200 m (grey) elevation contours

Figure S3: Percentage rainfall occurrence during the wettest 3-hr period.

Figure S4: Seasonal wind flows over Eastern Africa : meridional cross-section of 500 hPa wind direction (arrows pointing to the left denote easterly winds) and wind speed, along 35.25°E (a) and 44.25°E (b), and 925hPa streamlines for March-May (c), June-September (d) and October-December (e).

599 References

600

601 Anyah RO, Semazzi FH, Xie L. 2006. Simulated physical mechanisms associated with climate variability
602 over Lake Victoria Basin in East Africa. *Monthly Weather Review*, ***134***(12), 3588-3609.

603 Asnani GC, Kinuthia J.H., 1979: *Diurnal variation of precipitation in East Africa*. KMD Research
604 Report N°8/79, 58 pp.

605 Ba MB, Nicholson SE. 1998. Analysis of convective activity and its relationship to the rainfall over
606 the Rift Valley lakes of East Africa during 1983-90 using the METEOSAT infrared channel. *J.*
607 *Applied Met.,* **37**, 1250-1264.

608 Beltrando G 1990. Space–time variability of rainfall in April and October–November over East Africa
609 during the period 1932–1983. *International Journal of Climatology*, **10(7),** 691-702.

610 Biasutti M, Yuter SE, Burleyson CD, Sobel AH. 2012. Very high resolution rainfall patterns measured
611 by TRMM precipitation radar: seasonal and diurnal cycles. *Climate dynamics*, **39**(1-2), 239-258.

612 Camberlin P, Planchon O. 1997. Coastal precipitation regimes in Kenya. *Geografiska Annaler*, **79A**,
613 1-2, 109-119.

614 Carbone RE, Wilson JW, Keenan TD, Hacker JM. 2000. Tropical Island Convection in the Absence of
615 Significant Topography. Part I: Life Cycle of Diurnally Forced Convection. *Mon. Wea. Rev*., **128**,
616 3459–3480

617 Cattani E, Merino A, Levizzani V. 2016. Evaluation of monthly satellite-derived precipitation products
618 over East Africa. *J. Hydrometeor*., in press, doi: 10.1175/JHM-D-15-0042.1

619 Cautenet S, Rosset R. 1989. Numerical simulation of sea breezes with vertical wind shear during dry
620 season at Cape of Three Points, West Africa. *Mon.Wea. Rev.* **117**: 329–339.

621 Clarke RH. 1984. Colliding sea-breezes and the creation of internal atmospheric bore waves: two-
622 dimensional numerical studies. *Australian Meteorological Magazine*, **32**(4), 207-226.

623 Crosman ET, Horel JD. 2010. Sea and Lake Breezes: A Review of Numerical Studies. *Boundary-Layer*
624 *Meteorology*, **137**(1), 1−29. http://doi.org/10.1007/s10546-010-9517-9

625 Dai A. 2001. Global precipitation and thunderstorm frequencies. Part II: Diurnal variations. *Journal*
626 *of Climate*, **14**(6), 1112-1128.

627 Datta RR. 1981. Certain aspects of monsoonal precipitation dynamics over Lake Victoria. in
628 *Monsoon Dynamics*, Lighthill and Pearce, Eds. 333-349.

629 Davis SR, Pratt LJ, Jiang H. 2015. The Tokar Gap Jet: Regional Circulation, Diurnal Variability and
630 Moisture Transport based on Numerical Simulations. *Journal of Climate*, ***28***(15), 5885-5907.

631 Dee DP, Uppala SM, Simmons AJ, Berrisford P, Poli P, Kobayashi S, ... & Bechtold P. 2011. The ERA-
632 Interim reanalysis: Configuration and performance of the data assimilation system. *Quarterly*
633 *Journal of the royal meteorological society*, **137**(656), 553-597.

634 Desbois M, Kayiranga T, Gnamien B, Guessous S, Picon L. 1988. Characteristization of some
635 elements of the Sahelian climate and their interannual variations for July 1983, 1984 and
636 1985 from the analysis of METEOSAT ISCCP data. *J.of Climate*, **9**, 867-904.

637 Dhonneur G. 1985. *Traité de météorologie tropicale*. Météo-France, Paris, 151 pp.

638 El-Fandy MG. 1949. Forecasting the summer weather of the Sudan and the rains that lead to the Nile
639 floods. *Quarterly Journal of the Royal Meteorological Society*, ***75***(326), 375-398.

640 Flohn H, Fraedrich K. 1966. Tagesperiodische Zirkulation und Niederschlagsverteilung am Victoria-
641 See. *Meteor. Rundschau*, **6**, 157-165.

642 Funatsu B, Dubreuil V, Claud C, Arvor D, Gan MA. 2012. Convective activity in Mato Grosso State
643 (Brazil) from microwave satellite observations: Comparisons between AMSU and TRMM
644 datasets. *Journal of Geophysical Research,* (**177**) 1-16, doi:10.1029/2011JD017259

645 Garratt JR, Physick WL. 1985. The inland boundary layer at low latitudes: II Sea-breeze influences.
646 *Boundary-Layer Meteorology*, **33**(3), 209−231. http://doi.org/10.1007/BF00052056

647 Garstang M, Massie Jr HL, Halverson J, Greco S, Scala J. 1994. Amazon coastal squall lines. Part I:
648 Structure and kinematics*. Monthly Weather Review*, **122**(4), 608-622.

649 Haile AT, Rientjes T, Gieske A, Gebremichael M. 2009. Rainfall Variability over Mountainous and
650 Adjacent Lake Areas: The Case of Lake Tana Basin at the Source of the Blue Nile River. *J. Appl.*
651 *Meteor. Climatol.*, **48**, 1696–1717.

652 Haile AT, Habib E, Elsaadani M, Rientjes T. 2013. Inter-comparison of satellite rainfall products for
653 representing rainfall diurnal cycle over the Nile basin. *International journal of applied earth*
654 *observation and geoinformation*, ***21***, 230-240.

655 Hendon HH, Woodberry K. 1993. The diurnal cycle of tropical convection. *Journal of Geophysical*
656 *Research: Atmospheres,* **98**(D9), 16623-16637.

657 Holmes DA. 1972. Sea Breezes in West Pakistan. *Weather*, 27, 91-92.

658 Huffman GJ, Bolvin DT. 2013. *TRMM and other data precipitation data set documentation*. NASA,
659 Greenbelt, USA, 1-40.

660 Huffman GJ, Bolvin DT, Nelkin EJ, Wolff DB, Adler RF, Gu G, ... & Stocker EF. 2007. The TRMM
661 multisatellite precipitation analysis (TMPA): Quasi-global, multiyear, combined-sensor
662 precipitation estimates at fine scales. *Journal of Hydrometeorology*, **8**(1), 38-55.

663 Janowiak JE, Arkin PA, Morrissey M. 1994. An examination of the diurnal cycle in oceanic tropical
664 rainfall using satellite and in situ data. *Mon. Wea. Rev*., **122**, 10, 2296-2311.

665 Kayiranga T. 1991. Observation de l'activité convective à partir de données satellitaires sur la
666 région du lac Victoria en avril 1985. *Veille Climatique Satellitaire*, **37**, 44-55.

667 Kikuchi K, Wang B. 2008. Diurnal Precipitation Regimes in the Global Tropics. *Journal of Climate*
668 **21**:11, 2680-2696.

669 Kousky VE. 1980. Diurnal rainfall variation in northeast Brazil. *Monthly Weather Review*, **108**(4), 488-
670 498.

671 Laing AG, Carbone RE, Levizzani V. 2011. Cycles and propagation of deep convection over equatorial
672 Africa. *Monthly Weather Review*, ***139***(9), 2832-2853.

673 Laing AG, Carbone R, Levizzani V, Tuttle J. 2008. The propagation and diurnal cycles of deep
674 convection in northern tropical Africa. *Quarterly Journal of the Royal Meteorological Society*,
675 ***134***(630), 93-110.

676 Llasat MC, Puigcerver M. 1997. Total rainfall and convective rainfall in Catalonia, Spain. *International*
677 *Journal of Climatology*, **17**, 1683-1695.

678 Machado LA, Silva Dias MA, Morales C, Fisch G, Vila D, Albrecht R, ... & Cohen J. 2014. The Chuva
679 Project: How Does Convection Vary across Brazil? *Bulletin of the American Meteorological*
680 *Society*, **95**(9), 1365-1380.

681 McCollum JR, Ferraro RR. 2005. Microwave rainfall estimation over coasts*. J Atmos Oceanic Technol*
682 **22**, 497–512.

683 Meisner BN, Arkin PA. 1987. Spatial and annual variations in the diurnal cycle of large-scale tropical
684 convective cloudiness and precipitation. *Monthly weather review*, **115**(9), 2009-2032.

Miller STK, Keim BD, Talbot RW, Mao H. 2003. Sea breeze: Structure, forecasting, and impacts. *Rev. Geophys.,* **41**, 1011, doi:10.1029/2003RG000124, 3.

Molion LCB. 1987. On the dynamic climatology of the Amazon basin and associated rain-producing mechanisms. In: R. E. Dickinson (ed.), *The Geophysiology of Amazonia*, Wiley, 391–407.

Mori S, Jun-Ichi H, Tauhid YI, Yamanaka MD, Okamoto N, Murata F, … Sribimawati T. 2004. Diurnal Land–Sea Rainfall Peak Migration over Sumatera Island, Indonesian Maritime Continent, Observed by TRMM Satellite and Intensive Rawinsonde Soundings. *Monthly Weather Review*, **132**(8), 2021−2039. http://doi.org/10.1175/1520-0493(2004)132<2021:DLRPMO>2.0.CO;2

Mukabana JR, Pielke RA. 1996. Investigating the influence of synoptic-scale monsoonal winds and mesoscale circulations on diurnal weather patterns over Kenya using a mesoscale numerical model. *Mon. Wea. Rev.,* **124**, 224-243.

Nesbitt SW, Zipser EJ. 2003. The diurnal cycle of rainfall and convective intensity according to three years of TRMM measurements. *Journal of Climate*, **16**(10):1456-1475

Nganga JK, Masumba BAN. 1988. The land and sea breeze circulation and its influence on rainfall over Kenya's coastal areas. *WMO, T.M.R.P. Report Series* **28**, 220–221.

Nicholson SE, Yin X. 2002. Mesoscale patterns of rainfall, cloudiness and evaporation over the Great Lakes of Africa. In *The East African Great Lakes: Limnology, Palaeolimnology and Biodiversity*. E.O. Odada & D. O. Olago, eds. Kluwer Academic Publishers, Dordrecht, Netherlands, 93-120.

Okoola REA. 1978. Spatial distribution of precipitation in the Mombasa area of Kenya. Kenya Meteorological Department, *IMTR Research Report*, 1/78.

Paiva RCD, Buarque DC, Clarke RT, Collischonn W, Allasia DG. 2011. Reduced precipitation over large water bodies in the Brazilian Amazon shown from TRMM data. *Geophysical Research Letters*, **38**(4).

Pedgley DE. 1969. Diurnal variation of the incidence of monsoon rainfall over the Sudan. *Met. Mag.*, **98**, 97-106 and 129-134.

Pedgley DE. 1971. Diurnal incidence of rain and thunder at Asmara and Addis-Ababa. *Met. Mag.,* **100**, 66-71.

Pfeifroth U, Trentmann J, Fink AH, Ahrens B. 2016. Evaluating satellite-based diurnal cycles of precipitation in the African tropics. *Journal of Applied Meteorology and Climatology*, ***55***(1), 23-39.

Physick WL, Smith RK 1985. Observations and dynamics of sea-breezes in northern Australia. *Australian Meteorological Magazine*, **33**(2), 51-63.

Planchon O. 1995. Les variations diurnes de la direction du vent dans le Top End (Territoire du Nord, Australie). *Le Climat*, **13** (2), 11-26.

Planchon O, Damato F, Dubreuil V, Gouéry P. 2006. A method of identifying and locating sea-breeze fronts in north-eastern Brazil by remote sensing. *Meteorological Applications*, **13**(3), 225-234.

Rickenbach TM. 2004. Nocturnal Cloud Systems and the Diurnal Variation of Clouds and Rainfall in Southwestern Amazonia. *Monthly Weather Review*, **132**(5), 1201−1219. http://doi.org/10.1175/1520-0493(2004)132<1201:NCSATD>2.0.CO;2

Rientjes T, Haile AT, Fenta AA. 2013. Diurnal rainfall variability over the Upper Blue Nile Basin: A remote sensing based approach. *International Journal of Applied Earth Observation and Geoinformation*, **21**, 311-325. http://doi.org/10.1016/j.jag.2012.07.009

Sahany S, Venugopal V, Nanjundiah RS. 2010. Diurnal-scale signatures of monsoon rainfall over the Indian region from TRMM satellite observations. *J. Geophys. Res*., **115**, D02103, doi:10.1029/2009JD012644

Savijärvi H. 1997. Diurnal winds around Lake Tanganyika. *Quarterly Journal of the Royal Meteorological Society*, **123**, 901-918.

Shinoda M, Okatani T, Saloum M. 1999. Diurnal variations of rainfall over Niger in the West African Sahel: a comparison between wet and drought years. *International Journal of Climatology*, **19**(1), 81−94. http://doi.org/10.1002/(SICI)1097-0088(199901)19:1<81::AID-JOC350>3.0.CO;2-F

Snow JW. 1976. The climate of Northern South America. In: *World Survey of Climatology*, Elsevier Publishing Company, 12 (6), 295-403.

Steedman RA, Ashour Y. 1976. Sea breezes over north-west Arabia. *Tellus*, **28**, 4, 299-306.

Sumner GN. 1982. Rainfall and wind circulation in Coastal Tanzania. *Archives for meteorology, geophysics, and bioclimatology, Series B*, ***30***(1-2), 107-125.

Sumner GN. 1984. The impact of wind circulation on the incidence and nature of rainstorms over Dar es Salaam, Tanzania. *Journal of climatology*, ***4***(1), 35-52.

Takahashi HG, Fujinami H, Yasunari T, Matsumoto J. 2010. Diurnal rainfall pattern observed by Tropical Rainfall Measuring Mission Precipitation Radar (TRMM-PR) around the Indochina peninsula. *J. Geophys. Res*., **115**, D07109, doi:10.1029/2009JD012155

Teo CK, Koh TY, Chun-Fung Lo J, Chandra Bhatt B. 2011. Principal Component Analysis of Observed and Modeled Diurnal Rainfall in the Maritime Continent. *Journal of Climate*, **24**(17), 4662−4675. http://doi.org/10.1175/2011JCLI4047.1

Thiery W, Davin EL, Panitz HJ, Demuzere M, Lhermitte S, Van Lipzig N. 2015. The impact of the African Great Lakes on the regional climate. *Journal of Climate*, ***28***(10), 4061-4085.

Tian Y, Peters-Lidard CD. 2007. Systematic anomalies over inland water bodies in satellite-based precipitation estimates. *Geophysical Research Letters*, **34**(14), L14403. http://doi.org/10.1029/2007GL030787

Tomsett JE. 1975. *The diurnal variation of precipitation in East Africa.* EAMD Technical Memorandum n°25, 66 pp.

Yang GY, Slingo J. 2001. The diurnal cycle in the tropics. *Monthly Weather Review*, ***129***(4), 784-801.

Yang S, Smith EA. 2006. Mechanisms for diurnal variability of global tropical rainfall observed from TRMM. *J. Climate*, **19**, 5190–5226.

Yang S, Kuo KS, Smith EA. 2008. Persistent nature of secondary diurnal modes of precipitation over oceanic and continental regimes. *Journal of Climate*, ***21***(16), 4115-4131.

Yaodong L, Yun W, Yang S, Liang H, Shouting G, Fu R. 2008. Characteristics of Summer Convective Systems Initiated over the Tibetan Plateau. Part I: Origin, Track, Development, and Precipitation. *Journal of Applied Meteorology and Climatology*, **47**(10), 2679−2695. http://doi.org/10.1175/2008JAMC1695.1

Zhou L, Wang Y. 2006. Tropical Rainfall Measuring Mission observation and regional model study of precipitation diurnal cycle in the New Guinean region. *J. Geophys. Res*., **111**, D17104, doi:10.1029/2006JD007243.

Zhu M, Atkinson BW. 2004. Observed and modelled climatology of the land–sea breeze circulation over the Persian Gulf. *International Journal of Climatology*, **24**(7), 883−905. http://doi.org/10.1002/joc.1045

770 Zulkafli Z, Buytaert W, Onof C, Manz B, Tarnavsky E, Lavado W, Guyot JL. 2013. A Comparative
771 Performance Analysis of TRMM 3B42 (TMPA) Versions 6 and 7 for Hydrological Applications over
772 Andean–Amazon River Basins. *Journal of Hydrometeorology*, **15**(2), 581−592.
773 http://doi.org/10.1175/JHM-D-13-094.1

774

Figure Captions

Figure 1: Location map and relief of Eastern Africa (elevation in meters). 1: Lake Albert ; 2 : Lake Kyoga ; 3 : Lake Edward

Figure 2: 3-hour period during which precipitation is (a) most frequent and (b) most abundant, TRMM data (1998-2014, whole year). 3 EAT stands for the period between 0130 and 0430 East African Time. Arrows show the most apparent phase propagations (see text). Solid lines: 1000 (white) and 2200 m (grey) elevation contours. Areas where mean rainfall frequency does not exceed 0.5% in any 3-hr period (a) or mean annual rainfall is below 80 mm (b) are left blank. Central histogram: percentage of grid-points as a function of the 3-hour period during which rainfall is most frequent (in red: land grid-points only)

Figure 3: Same as Fig.2a but for the region covering Sudan, South Sudan, western Ethiopia and western Eritrea. Dots indicate a secondary maximum at 1500 or 1800 EAT. White lines: 800 and 1500 m contour lines. Side panels: percentage of all local rainfall occurrences in each 3-hour period at the stations located on map, with bars showing TRMM data and blue lines showing in situ rainfall records (period 1951-1966, depending on stations ; Pedgley, 1969 and 1971).

Figure 4: Same as Fig.2b but for the region covering Kenya, Tanzania, Uganda, Rwanda and Burundi. White lines: 700 and 1400 m contour lines. Pluses: over 35% of total precipitation recorded in the wettest 3-hr period. Side panels: percentage of rainfall amounts in each 3-hour period at stations located by squares, with bars showing TRMM data and blue lines showing in situ rainfall records (6- to 26-yr averages, depending on stations; Tomsett, 1975).

Figure 5: Same as Fig.2b but for Somalia and south-eastern Ethiopia. White lines: 500 and 1000 m contour lines. Side panels: percentage of rainfall amounts in each 3-hour period at stations located by squares, with bars showing TRMM data and blue lines in situ rainfall records (SWALIM stations) for the period 2008-2015 depending on stations (only 2 years are available for Burao and Galcaio).

Figure 6: Raw rainfall occurrence for each 3-hour period, all months together (average for 1998-2014). White contours : over 25%.

Figure 7: Rainfall occurrence in each 3-hour period, as a percentage of all local rainfall occurrences, all months together. Areas where the maximum raw rainfall occurrence over any 3-hr period does not exceed 0.5% are left blank.

Figure 8: Time-longitude plot of diurnal rainfall occurrence along 1.5°S. Top : elevation cross-section. Bottom : percentage of local rainfall occurrence during each 3-hr period. For convenience, two consecutive diurnal cycles are plotted. Heavy grey lines show approximate propagation and corresponding speeds.

Figure 9: Time-longitude plot of diurnal rainfall occurrence along 15°N. Top : elevation cross-section. Bottom : percentage of local rainfall occurrence during each 3-hr period. For convenience, two consecutive diurnal cycles are plotted.

Figure 10: Distribution of rainfall in each 3-hr period (percentage of total rainfall occurrences at each location) as a function to the inland distance to the nearest coastline (12°S to 23°N). From left to right : Annual average, April, July, October. Plots show two consecutive diurnal cycles.

Figure 11: Mean diurnal rainfall regimes over the main lakes of Eastern Africa, ordered according to their size. Colours refer to the wettest 3-hr period, as in figure 2. Bars use all grid-points having at least 25 % of lake surface, and lines with stars use grid-points having over 75% of lake surface (larger lakes only). Captions indicate the mean altitude of the lake surface and the total surface area considered in the computation, which may slightly differ from actual lake sizes due to TRMM data resolution. Last panel: averages for all lakes, with the dashed line and squares showing the corresponding cycle for all land grid-points.

Figure 12: Percentage of local daily rainfall in each 3-hr period, for lake and non-lake (sea and land) pixels. Lake pixels are stratified according to the distance to the nearest shore (i.e., full land pixel).

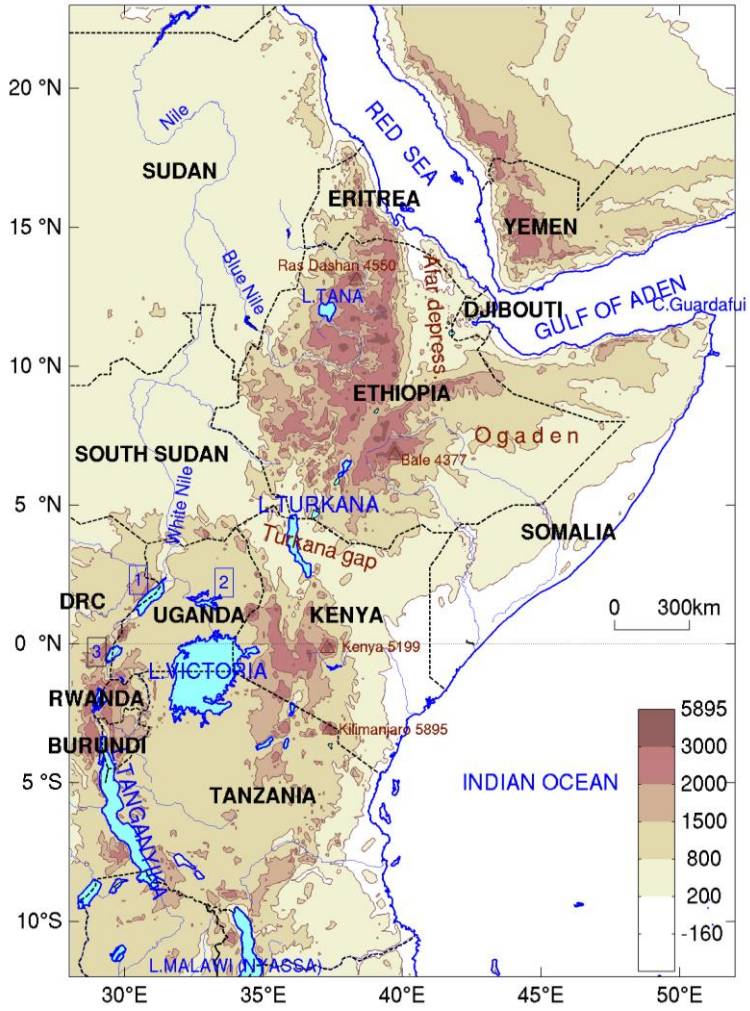

Figure 1: Location map and relief of Eastern Africa (elevation in meters).
1: Lake Albert ; 2 : Lake Kyoga ; 3 : Lake Edward

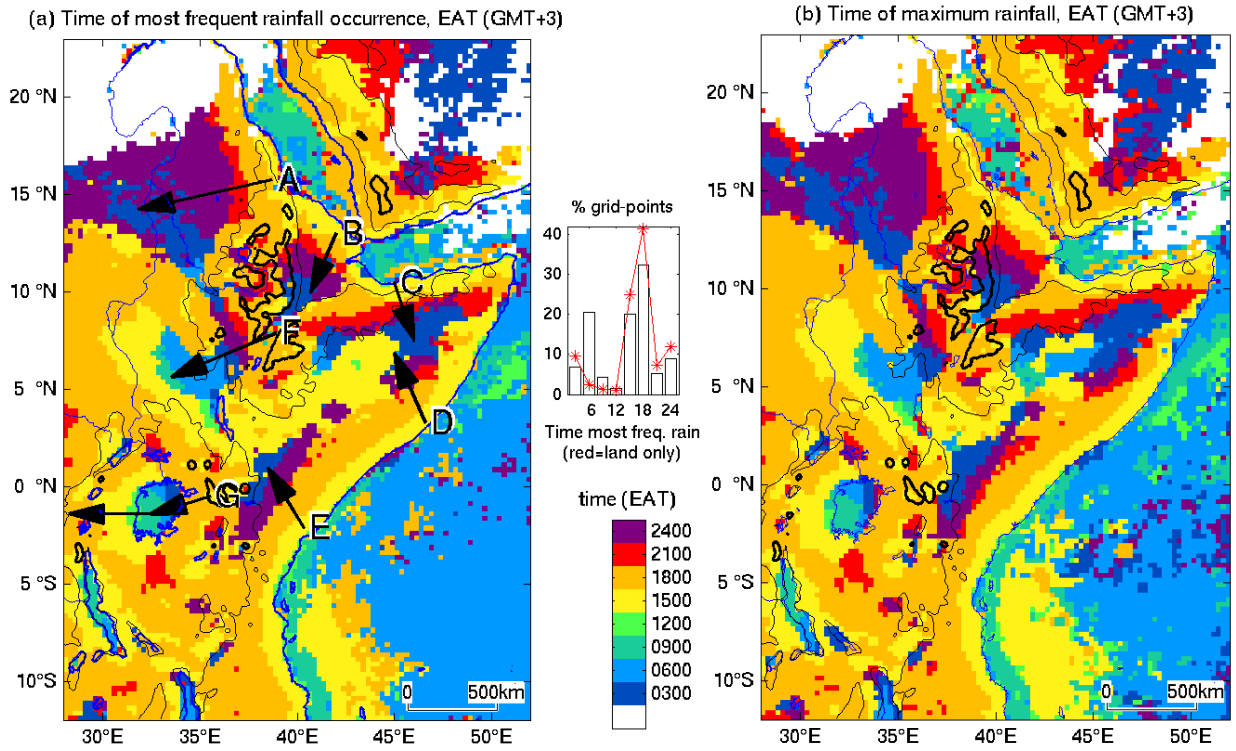

Figure 2: 3-hour period during which precipitation is (a) most frequent and (b) most abundant, TRMM data (1998-2014, whole year). 3 EAT stands for the period between 0130 and 0430 East African Time. Arrows show the most apparent phase propagations (see text). Black lines: 1000 m (thin) and 2200 m (thick) elevation contours. Areas where mean rainfall frequency does not exceed 0.5% in any 3-hr period (a) or mean annual rainfall is below 80 mm (b) are left blank. Central histogram: percentage of grid-points as a function of the 3-hour period during which rainfall is most frequent (in red: land grid-points only)

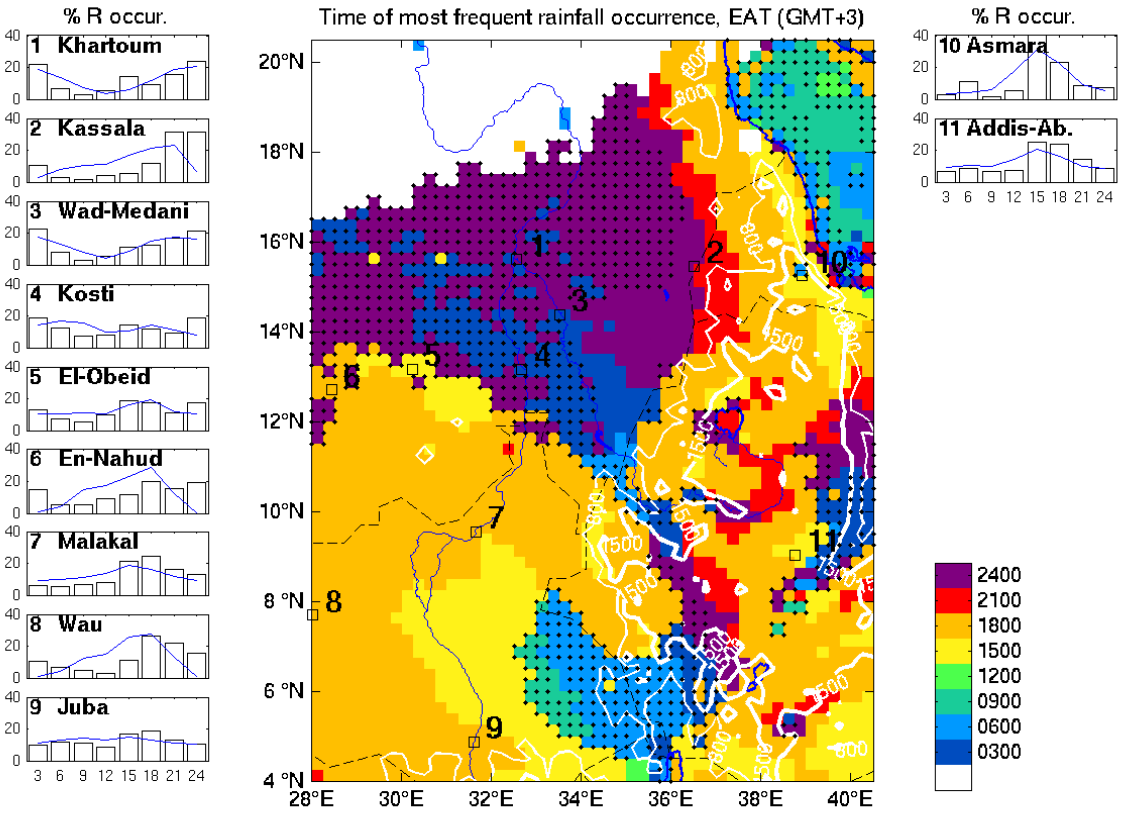

838
839 Figure 3: Same as Fig.2a but for the region covering Sudan, South Sudan, western Ethiopia and western Eritrea.
840 Dots indicate a secondary maximum at 1500 or 1800 EAT. White lines: 800 and 1500 m contour lines. Side
841 panels: percentage of all local rainfall occurrences in each 3-hour period at the stations located on map, with
842 bars showing TRMM data and blue lines showing in situ rainfall records (period 1951-1966, depending on
843 stations ; Pedgley, 1969 and 1971).
844

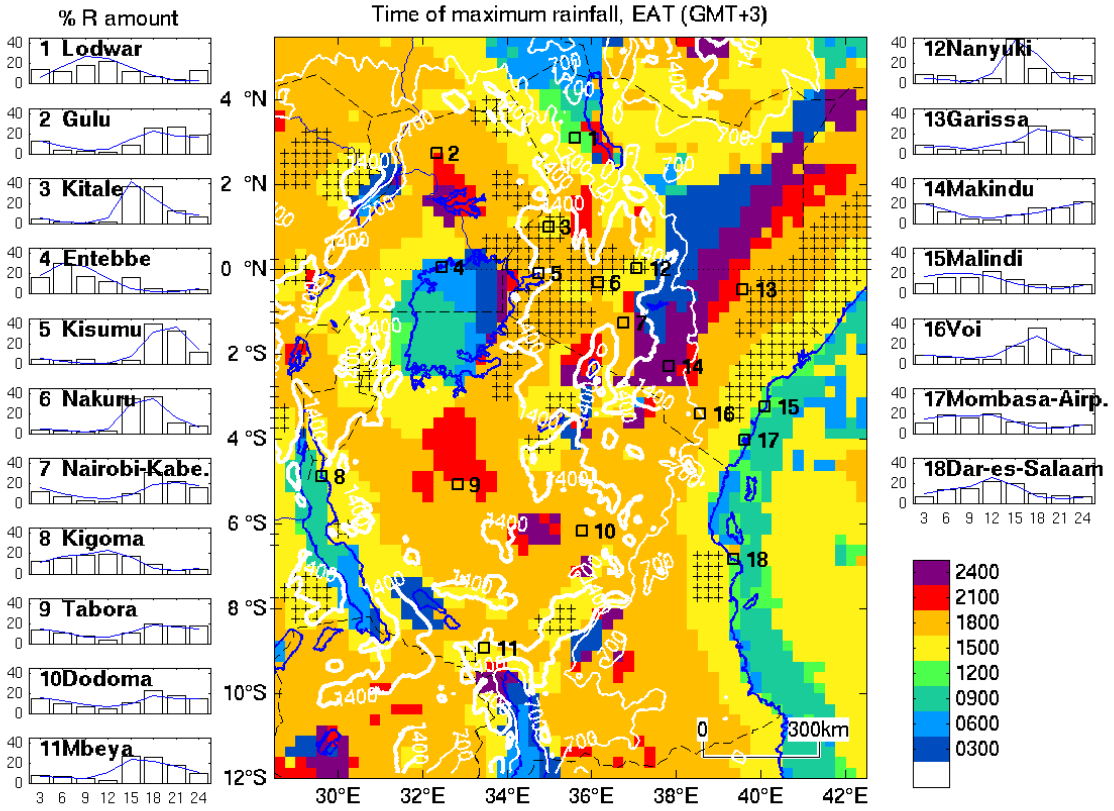

Figure 4: Same as Fig.2b but for the region covering Kenya, Tanzania, Uganda, Rwanda and Burundi. White lines: 700 and 1400 m contour lines. Pluses: over 35% of total precipitation recorded in the wettest 3-hr period. Side panels: percentage of rainfall amounts in each 3-hour period at stations located by squares, with bars showing TRMM data and blue lines showing in situ rainfall records (6- to 26-yr averages, depending on stations; Tomsett, 1975).

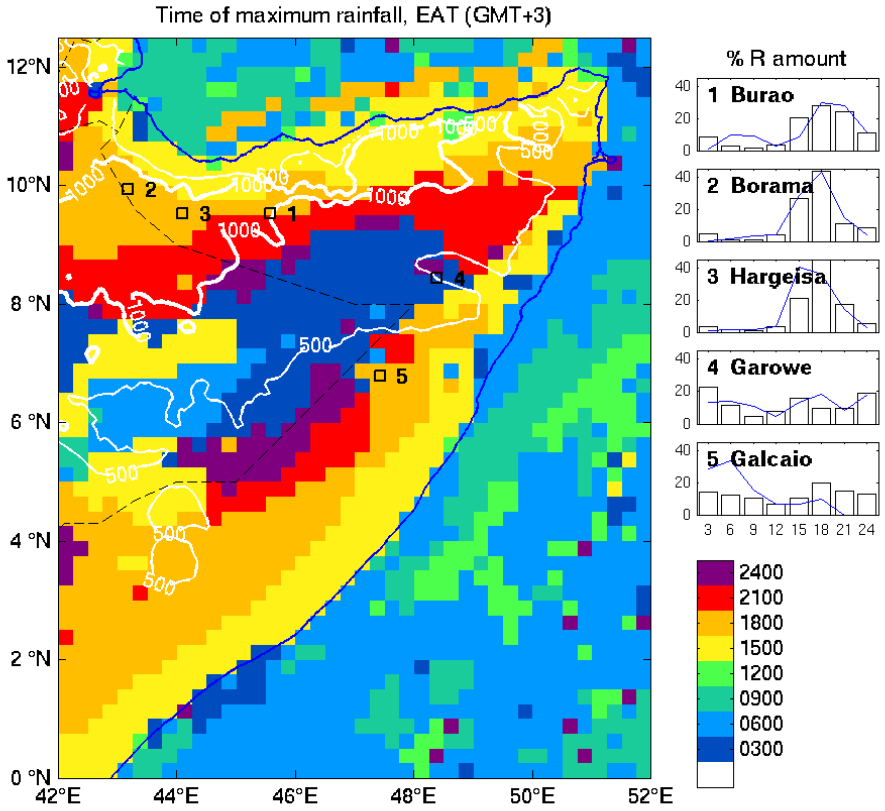

Figure 5: Same as Fig.2b but for Somalia and south-eastern Ethiopia. White lines: 500 and 1000 m contour lines. Side panels: percentage of rainfall amounts in each 3-hour period at stations located by squares, with bars showing TRMM data and blue lines in situ rainfall records (SWALIM stations) for the period 2008-2015 depending on stations (only 2 years are available for Burao and Galcaio).

Figure 6 : Raw rainfall occurrence for each 3-hour period, all months together (average for 1998-2014). Black lines: 1000 m (thin) and 2200 m (thick) elevation contours.

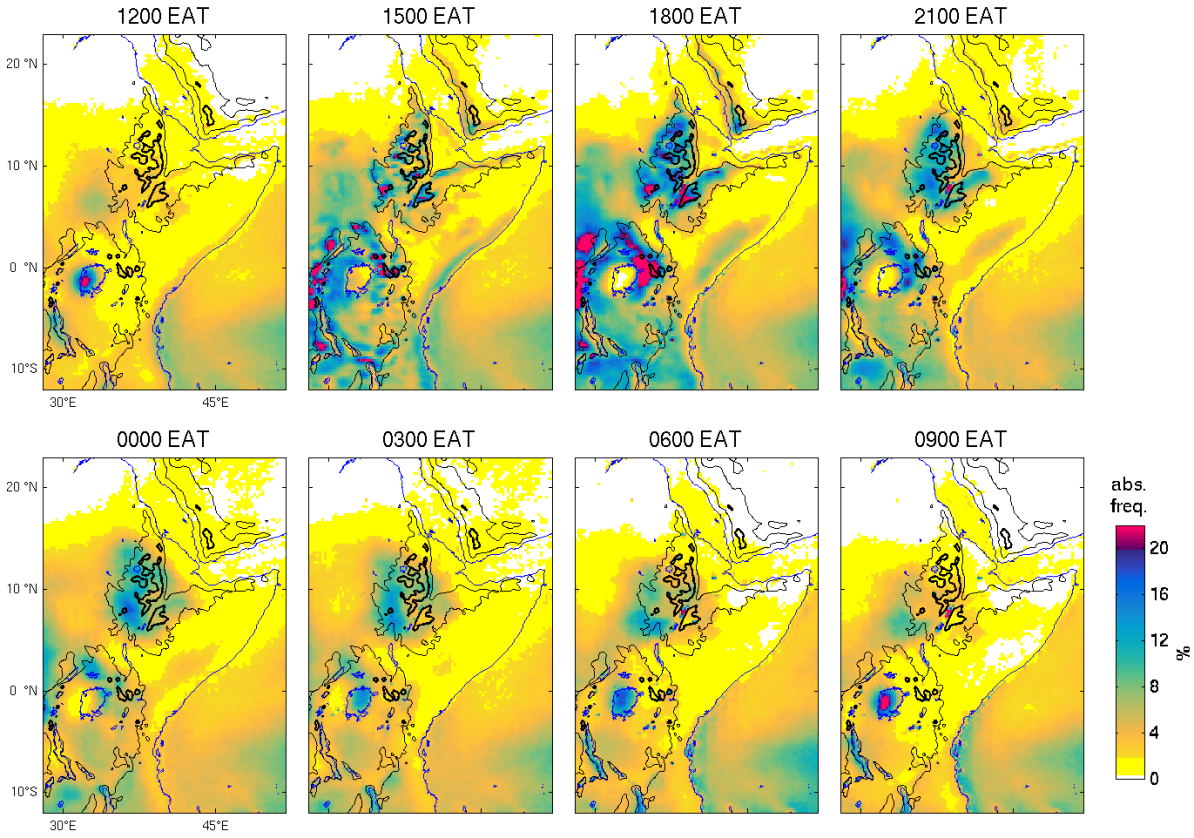

Figure 7 : Rainfall occurrence in each 3-hour period, as a percentage of all local rainfall occurrences, all months together. Areas where the maximum raw rainfall occurrence over any 3-hr period does not exceed 0.5% are left blank. Black lines: 1000 m (thin) and 2200 m (thick) elevation contours.

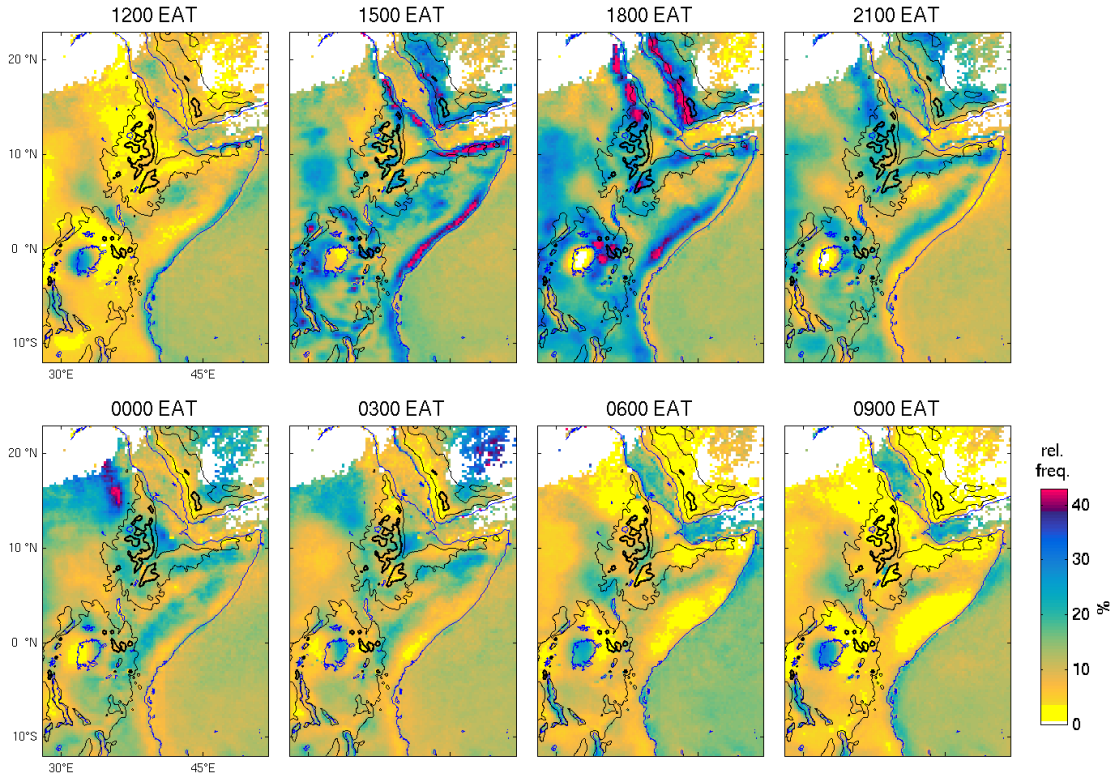

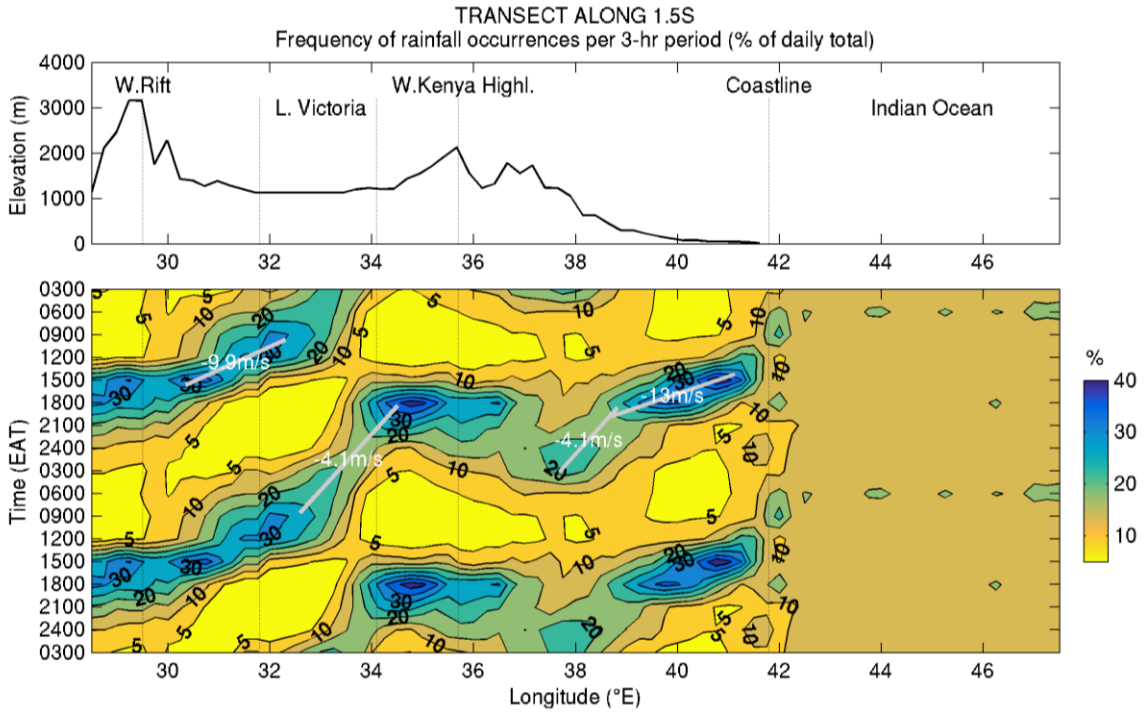

Figure 8: Time-longitude plot of diurnal rainfall occurrence along 1.5°S. Top : elevation cross-section. Bottom : percentage of local rainfall occurrence during each 3-hr period. For convenience, two consecutive diurnal cycles are plotted. Heavy grey lines show approximate propagation and corresponding speeds.

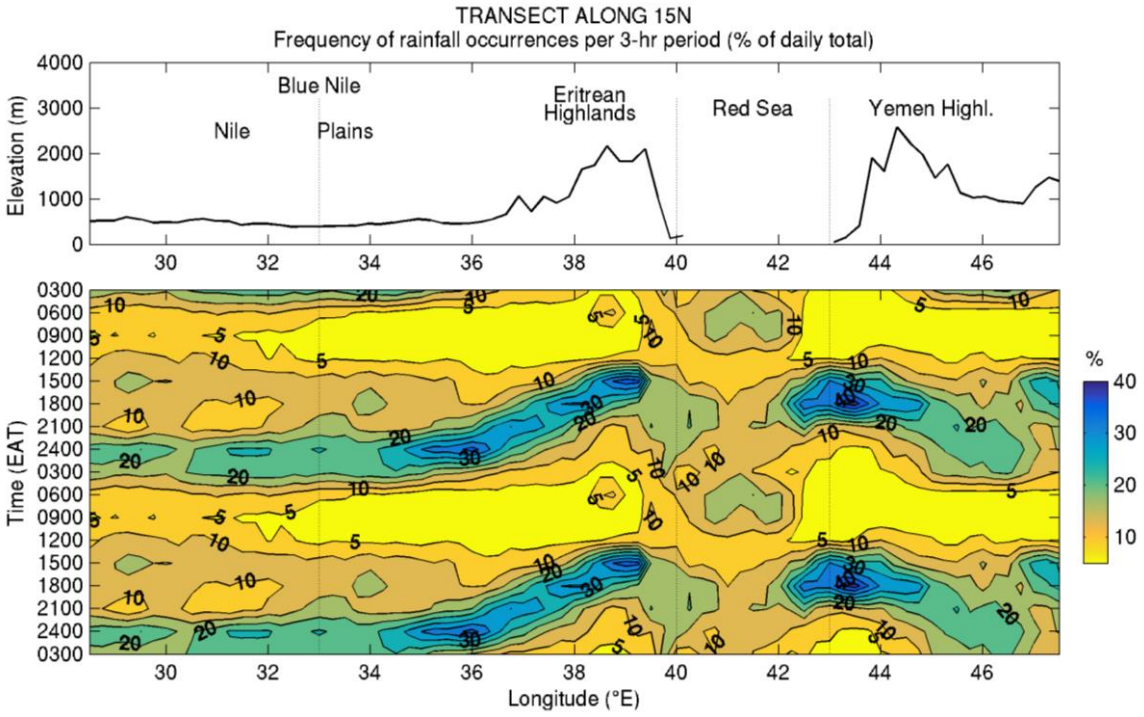

Figure 9 : Time-longitude plot of diurnal rainfall occurrence along 15°N. Top : elevation cross-section. Bottom : percentage of local rainfall occurrence during each 3-hr period. For convenience, two consecutive diurnal cycles are plotted.

881

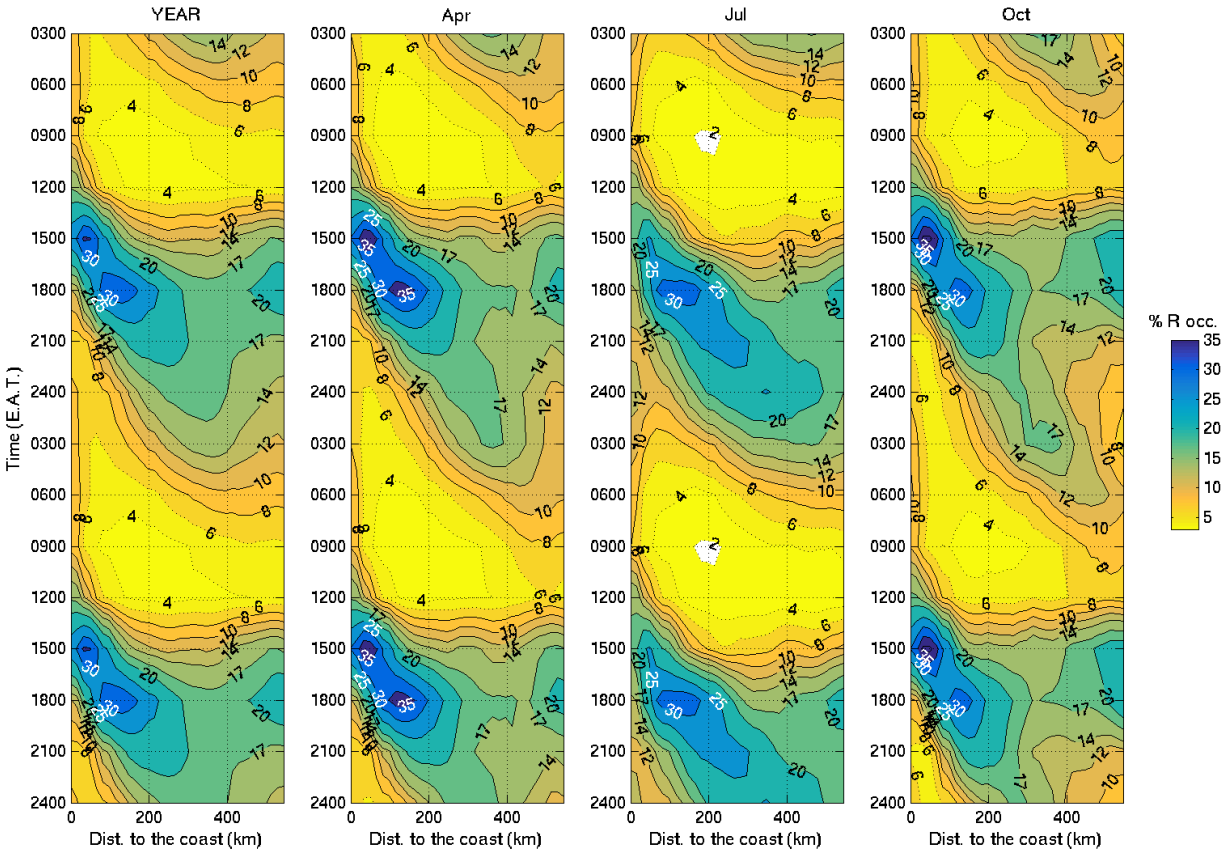

882
883

884 Figure 10 : Distribution of rainfall in each 3-hr period (percentage of total rainfall occurrences at each location)
885 as a function to the inland distance to the nearest coastline (12°S to 23°N). From left to right : Annual average,
886 April, July, October. Plots show two consecutive diurnal cycles.

887
888

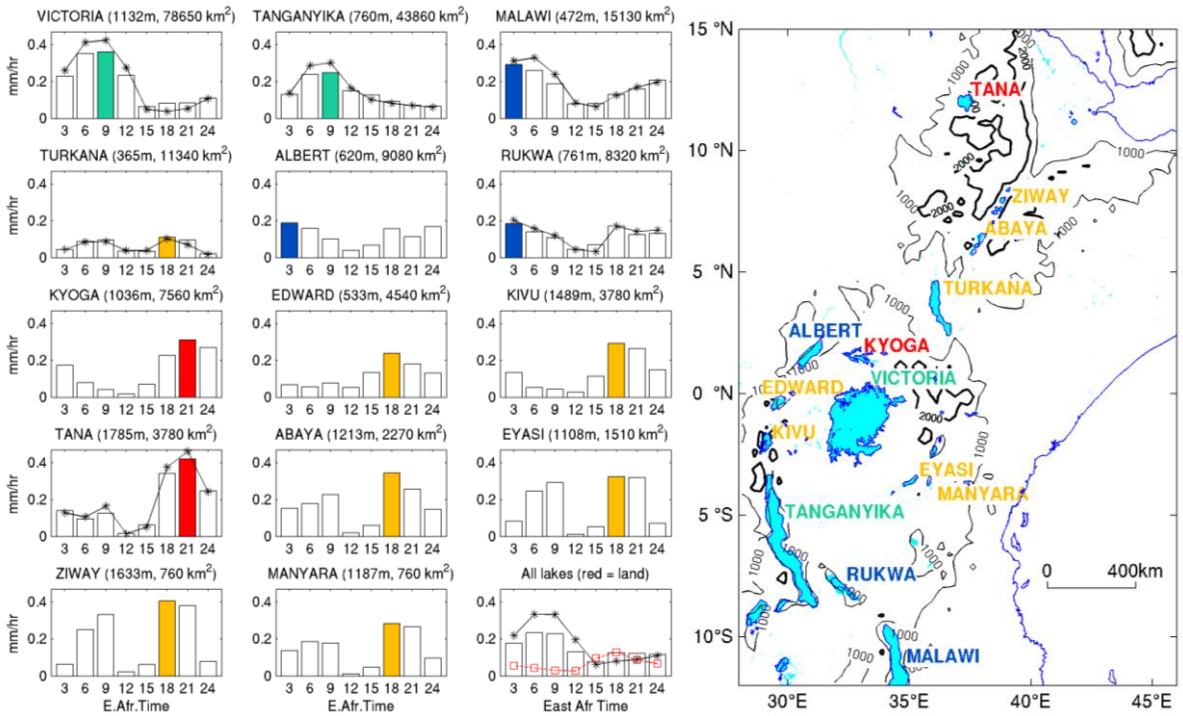

889

890
891 Figure 11 : Mean diurnal rainfall regimes over the main lakes of Eastern Africa, ordered according to their size.
892 Colours refer to the wettest 3-hr period, as in figure 2. Bars use all grid-points having at least 25 % of lake
893 surface, and lines with stars use grid-points having over 75% of lake surface (larger lakes only). Captions
894 indicate the mean altitude of the lake surface and the total surface area considered in the computation, which
895 may slightly differ from actual lake sizes due to TRMM data resolution. Lower right panel: averages for all lakes,
896 with the red line and squares showing the corresponding cycle for all land grid-points. Right panel: location
897 map; black lines: 1000 (thin) and 2200 m (thick) elevation contours.
898

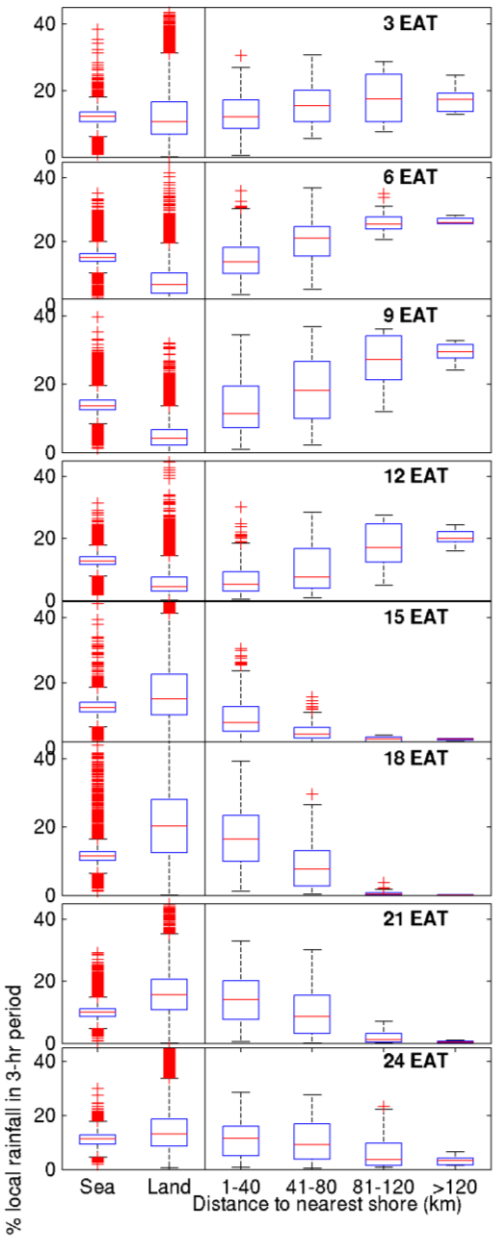

Figure 12 : Percentage of local daily rainfall in each 3-hr period, for lake and non-lake (sea and land) pixels. Lake pixels are stratified according to the distance to the nearest shore (i.e., full land pixel).